Report

Current Biology

A new Cambrian stem-group echinoderm reveals the evolution of the anteroposterior axis

Graphical abstract

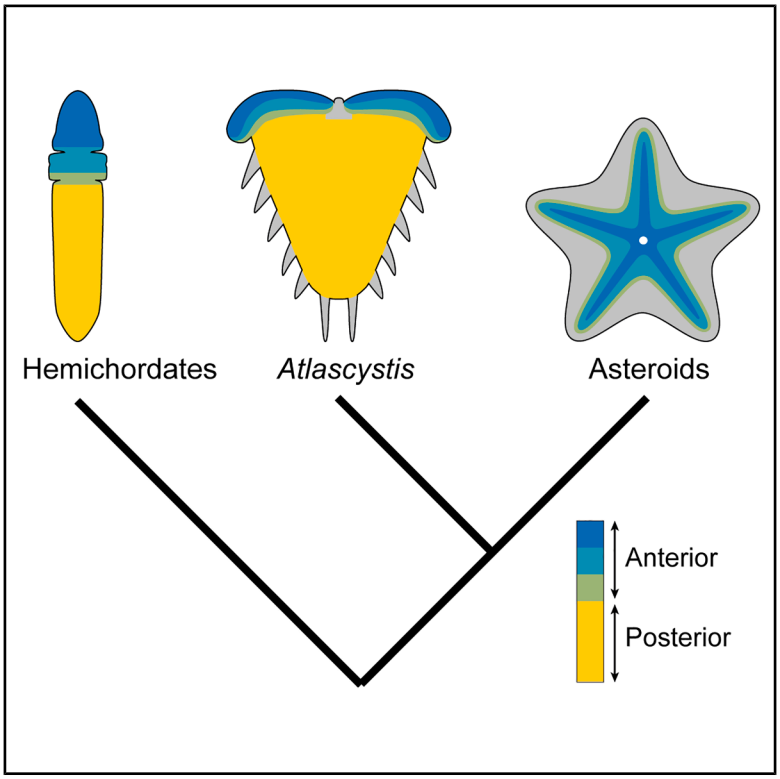

Authors

Stephanie C. Woodgate, Frances S. Dunn, Jeffrey R. Thompson, Laurent Formery, Samuel Zamora, Imran A. Rahman

Correspondence

s.zamora@igme.es (S.Z.), imran.rahman@nhm.ac.uk (I.A.R.)

In brief

Woodgate et al. describe a new bilaterally symmetrical echinoderm, *Atlascystis acantha*, from the Cambrian of Morocco. Comparisons of plate growth with other echinoderms reveal that *Atlascystis* possessed ambulacra. *Atlascystis* is recovered as an early stem-group echinoderm, revealing how pentaradial symmetry evolved from a bilateral ancestor.

Highlights

- We describe the oldest bilaterally symmetrical echinoderm, *Atlascystis acantha*
- *Atlascystis* possessed ambulacra, establishing homologies with other echinoderms
- Phylogenetic analyses recover *Atlascystis* as a stem echinoderm
- We uncover the early evolution of the echinoderm anteroposterior axis

Woodgate et al., 2025, Current Biology *35*, 1–8
July 21, 2025
https://doi.org/10.1016/j.cub.2025.05.065

CellPress

Current Biology

CellPress
OPEN ACCESS

Report

A new Cambrian stem-group echinoderm reveals the evolution of the anteroposterior axis

Stephanie C. Woodgate,[1,2] Frances S. Dunn,[3] Jeffrey R. Thompson,[4,5] Laurent Formery,[6,7] Samuel Zamora,[8,9,*] and Imran A. Rahman[3,10,11,*]

[1]Museum für Naturkunde, Leibniz-Institut für Evolutions- und Biodiversitätsforschung, 10115 Berlin, Germany
[2]Institute of Biology, Faculty of Life Sciences, Humboldt-Universität zu Berlin, 10115 Berlin, Germany
[3]Oxford University Museum of Natural History, University of Oxford, Oxford OX1 3PW, UK
[4]School of Biological Sciences, University of Southampton, Southampton SO17 1BJ, UK
[5]School of Ocean and Earth Science, University of Southampton, Southampton SO14 3ZH, UK
[6]Department of Biology, Hopkins Marine Station, Stanford University, Pacific Grove, CA 93950, USA
[7]Department of Molecular and Cell Biology, University of California, Berkeley, Berkeley, CA 94720, USA
[8]Instituto Geológico y Minero de España (IGME-CSIC), 50006 Zaragoza, Spain
[9]Grupo Aragosaurus-IUCA, Universidad de Zaragoza, 50009 Zaragoza, Spain
[10]The Natural History Museum, London SW7 5BD, UK
[11]Lead contact
*Correspondence: s.zamora@igme.es (S.Z.), imran.rahman@nhm.ac.uk (I.A.R.)
https://doi.org/10.1016/j.cub.2025.05.065

SUMMARY

Echinoderms are among the most morphologically distinctive animal phyla, encompassing familiar forms like starfish and sea urchins. Uncovering how their unique pentaradial body plan evolved from a bilaterally symmetrical ancestor has long proved challenging, as this involved fundamental changes to adult morphology and body plan development, associated with a complete reorganization of the anteroposterior (A-P) axis,[1–3] obfuscating homologies between disparate groups.[4,5] This has greatly limited our understanding of one of the most radical transformations in bilaterian evolutionary history.[6–8] Here, we describe a new bilaterally symmetrical echinoderm, *Atlascystis acantha*, from the Cambrian of Morocco.[9] This is the oldest bilaterally symmetrical echinoderm and the first with this body plan known from different ontogenetic stages, allowing us to elucidate mechanisms of its growth. This demonstrates that *Atlascystis* possessed ambulacra—structures accommodating extensions of the characteristic echinoderm water vascular system—providing a clear point of homology between *Atlascystis* and radially symmetrical forms. By integrating the Cambrian fossil record and our new phylogeny with developmental biology,[10] we uncover how changes to the ancestral bilaterian A-P patterning network alongside stepwise morphological transformations gave rise to the pentaradial structure of extant echinoderms, transforming our understanding of the origin and earliest evolution of this major animal phylum.

RESULTS

Systematic paleontology

Echinodermata Bruguière, 1791 (ex Klein, 1734)
Ctenocystoidea Robison & Sprinkle, 1969
Atlascystis acantha gen. et sp. nov.
Figures 1, S1, and S2
2013 ctenocystoid gen. et sp. nov. 1 Smith et al.: p. 5, Figure 4F
2014 Cambrian ctenocystoid Zamora and Rahman: p. 1,107, Figure 1B
2015 undescribed ctenocystoid Rahman et al.: p. 40, Figure 1C
2024 Cambrian echinoderm Rahman and Zamora: p. 297, Figure 1F

Diagnosis

Ctenocystoid with a flattened, sub-triangular theca without a complete marginal frame. Ctenidium with a sub-triangular suroral plate and four centrally positioned suboral plates. Dorsal surface of the theca composed of ridged tessellate plates with large lateral spines. Two long posterior spines.

Etymology

Generic name derived from Atlas, in reference to the mountain range where the taxon occurs, and the Latin *cystis* (bladder). Species name from the Latin *acantha* (thorny and spiny), referring to the large spines at the margins of the theca.

Type material

Holotype: Natural History Museum, London (NHMUK) EE 19394, a complete, articulated specimen (part and counterpart) preserved as a mold in shale (Figures 1A–1C, 1E–1G, and S1). Paratypes: NHMUK EE 15319, 15324a, 15325, 15428, and 19395–19399 preserved as molds in shales (Figures 1D and S2).

Horizon and locality

Brèche à Micmacca Member, Jbel Wawrmast Formation, Agdzian regional stage,[11] corresponding approximately to the stage

Please cite this article in press as: Woodgate et al., A new Cambrian stem-group echinoderm reveals the evolution of the anteroposterior axis, Current Biology (2025), https://doi.org/10.1016/j.cub.2025.05.065

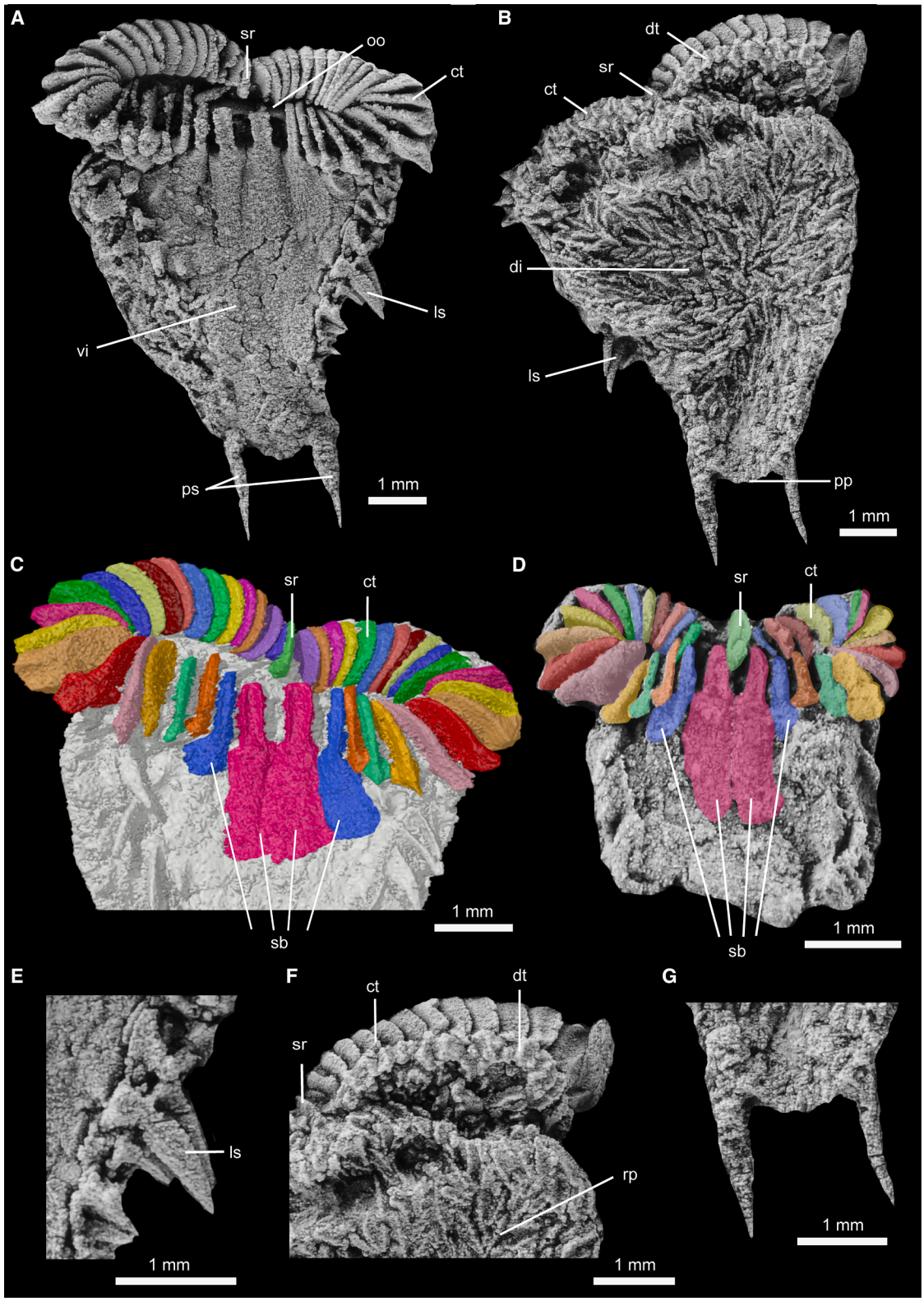

Figure 1. *Atlascystis acantha* from the Cambrian stage 4–Wuliuan boundary interval of Morocco
(A–C and E–G) NHMUK EE 19394.
(A and B) Ventral and dorsal views, respectively, of the complete specimen.
(C) Ctenidium and anterior theca in ventral view, with ctenidial plates highlighted.

(legend continued on next page)

4–Wuliuan boundary interval, Cambrian Series 2–Miaolingian.[12] Assemame (31.28768°N, 4.98493°W) and Tarhouch 3 (31.394 59°N, 5.01977°W) localities, Anti-Atlas, Morocco.[9,13]

Description

The theca is bilaterally symmetrical, dorsoventrally flattened, and sub-triangular in outline (Figures 1, S1, and S2). It ranges in size from approximately 3.3 to 9.9 mm in length and 2.9 to 8.1 mm in width (see Table S1 for additional measurements). The theca is fully plated and composed of dorsal and ventral integuments, with the ctenidium situated at the anterior (Figures 1A–1D, 1F, S1A, S1B, and S2A–2F) and a pair of long spines at the posterior (Figures 1A, 1B, and 1G).

The ctenidium is composed of a bilaterally symmetrical ring of radially orientated plates (the suroral plate, the suboral plates, and the ctenoid plates), which are differentiated in size and shape (Figures 1A–1D, S1A, S1B, and S2A–2F). Together, these plates frame a wide central opening (Figures 1A, 1C, 1D, S1A, S1B, S2B, and S2E). At the middle of the dorsal surface of the ctenidium, there is a sub-triangular suroral plate, which consists of an elongate blade-like process and a wide base (Figures 1A–1D, 1F, S1A–S1D, and S2B). This articulates with the first pairs of ctenoid plates and the dorsal integument. There are four suboral plates (M0l, M0r, M1l, and M1r), each of which consists of an anterior blade-like process with a central furrow and a large flattened posterior base located at the middle of the ventral ctenidium, and these articulate with each other, the adjacent ctenoid plates, and the ventral integument (Figures 1A, 1C, 1D, S1A, S1B, S2B, S2E, S2G, and S2H). M0l and M0r are centrally positioned. M1l and M1r articulate with M0l/r and the rest of the ventral integument. There are between 28 and 39 ctenoid plates preserved across the known specimens, with these plates arranged into symmetrical left and right sets located on either side of the suroral plate (Figures 1A–1D, 1F, S1A, S1B, and S2A–S2F; Table S1). The ctenoid plates are blade-like (Figures S1E and S1F), with the ventrolateral plates also possessing a prominent rectangular to pointed posterior base (Figure S1F).

The dorsal integument consists of numerous ridged polygonal tessellate plates (Figures 1B, 1F, S2A, S2C, S2D, and S2F). At the anterior, these are organized into a row of up to approximately 34 small polygonal plates, which extend from either side of the suroral plate to the lateral margins of the dorsal ctenidium and articulate anteriorly with the ctenoid plates (Figures 1F and S2A). The ventral integument is composed of thin, irregular polygonal plates, which form a tessellated surface (Figures 1A, S2B, and S2E). Rows of large, curved, spinose elements occur on the lateral margins of the theca, forming an incomplete ring around the body, and these marginal spines have an expanded proximal base and taper distally (Figures 1A, 1B, 1E, S2D, and S2E). At the posterior of the theca, there is a pair of long, pointed spines situated on either side of several small, elongate plates (Figures 1B, 1G, and S2A), which might represent the periproct.

Remarks

NHMUK EE 15428 was originally figured by Smith et al.,[9] who left it in open nomenclature as ctenocystoid gen. et sp. nov. 1. *Atlascystis acantha* is distinguished from other ctenocystoids by a combination of characters including the absence of a complete marginal frame, the presence of large lateral and posterior spines, and the morphology of the ctenidium.

Plate growth

To assess the hypothesized homology of the ctenocystoid ctenidium with echinoderm ambulacra,[14–16] we compared growth patterns for the ctenoid plates of *Atlascystis acantha* and the weakly asymmetrical ctenocystoid *Ctenocystis utahensis* with the ambulacral plates of the extant echinoid *Austrocidaris canaliculata* and the extant asteroid *Pisaster giganteus* (Figure S3). In echinoderms, ambulacra grow via the terminal addition of plates in rays (i.e., the ocular plate rule).[17] This process follows the von Bertalanffy function (a modified logistic function that has been used to model size-age relationships across animals[18,19]), with the size of individual plates increasing with time since their initial nucleation[20] and thus with distance from the growth zone. In all four echinoderms, the size of the plates generally increases with distance from the growth zone (adjacent to the suroral plate in the ctenocystoids, the ocular plates in the echinoid, and the terminal podia in the asteroid) (Figure 2). Plate growth for all the taxa fitted a von Bertalanffy curve with an adjusted R-squared value > 0.5 (Figure 2; Table S2), consistent with a general trend of increasing plate size with post-metamorphic age and indicating a common mode of growth.

Phylogenetic analyses

To determine the phylogenetic position of *Atlascystis acantha*, we carried out Bayesian analyses of a bilaterian character matrix. The bilaterally symmetrical fossil *Ctenoimbricata spinosa* was recovered as sister to all other echinoderms, with *Atlascystis* intermediate in position between this genus and a clade consisting of asymmetrical (*Ctenocystis utahensis*, *Trochocystites bohemicus*, *Protocinctus mansillaensis*, and *Coleicarpus sprinklei*), triradial (*Helicoplacus gilberti*), and pentaradial forms (Figures 3A and S4A). The edrioasteroids *Kailidiscus chinensis* and *Stromatocystites pentangularis* were recovered as sister to a clade of the pelmatozoans *Gogia spiralis*, *Metacrinus rotundus*, and *Tatonkacystis codyensis*. This topology was not affected by the choice of how to model rate variation (Figure S4B). The exclusion of discrete molecular characters led to the recovery of *Kailidiscus* and *Stromatocystites* in a polytomy with pelmatozoans and

(E) Lateral spines in ventral view.
(F) Right ctenidium and anterior theca in dorsal view.
(G) Posterior spines in ventral view.
(D) NHMUK EE 15324a(1). Ventral view of the complete specimen, with ctenidial plates highlighted.
(A, B, and D–G) Latex casts whitened with NH_4Cl sublimate. (C) Virtual reconstruction.
ct, ctenoid plate; di, dorsal integument; dt, dorsal tessellate plates; ls, lateral spine; oo, oral opening; pp, periproct; ps, posterior spines; rp, ridged plates; sb, suboral plates; sr, suroral plate; and vi, ventral integument.
See also Figures S1 and S2.

Please cite this article in press as: Woodgate et al., A new Cambrian stem-group echinoderm reveals the evolution of the anteroposterior axis, Current Biology (2025), https://doi.org/10.1016/j.cub.2025.05.065

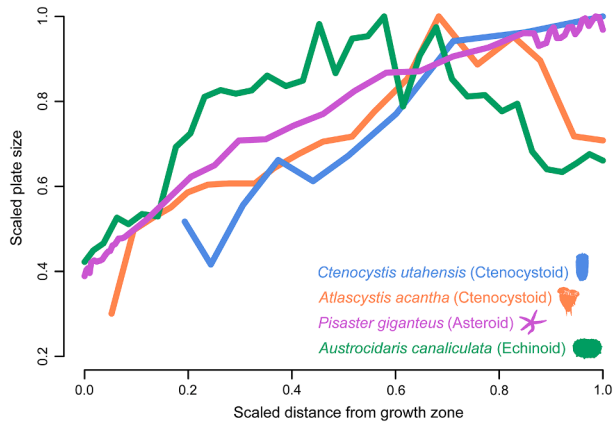

Figure 2. Plate growth in *Atlascystis* and other echinoderms

Plot showing scaled plate size against scaled distance from the growth zone for *Atlascystis acantha* and other extinct (*Ctenocystis utahensis*) and extant (*Austrocidaris canaliculata* and *Pisaster giganteus*) echinoderms. Adjusted R-squared values for fit to a von Bertalanffy function: *A. acantha*, 0.755; *C. utahensis*, 0.909; *A. canaliculata*, 0.582; and *P. giganteus*, 0.997.
See also Figure S3, Table S2, and Data S1.

eleutherozoans (*Pisaster giganteus*, *Amphiura filiformis*, *Austrocidaris canaliculata*, and *Apostichopus japonicus*) but did not influence the placement of any other fossil taxa (Figure S4C). The consensus network summarizing the posterior distribution of trees from our main analyses revealed minimal uncertainty in the phylogenetic relationships of extant and extinct echinoderms, with ctenocystoids and cinctans consistently recovered as early stem-group echinoderms (Figure S4D). Our topology was very strongly supported ($2 \times \log_e$ BF = 28) over an alternative hypothesis[16] in which the bilaterally symmetrical and asymmetrical forms were placed with the extinct pentaradial taxa *Gogia* and *Tatonkacystis*.

Ancestral state reconstructions (Figure 3A) indicate the presence of a hydrovascular system of tentacles in the most recent common ancestor of echinoderms (probability of presence = 0.87), with this system constructed from the left hydrocoel only in the most recent common ancestor of *Coleicarpus* and radial echinoderms (probability of presence = 1.00). Our analyses were equivocal as to whether ambulacra were present in the most recent common ancestor of echinoderms (probability of presence = 0.50), but this character was present in the most recent common ancestor of *Atlascystis* and non-bilateral echinoderms (probability of presence = 1.00). We reconstruct the presence of two ambulacra in the most recent common ancestors of *Atlascystis* and non-bilateral echinoderms (probability of presence = 0.99) and cinctans, *Coleicarpus*, and radial echinoderms (probability of presence = 0.92), with one ambulacrum present in the most recent common ancestor of *Coleicarpus* and radial echinoderms (probability of presence = 0.74).

DISCUSSION

Our results support the interpretation of the ctenocystoid ctenidium as a pair of recumbent ambulacra converging at a central mouth.[14–16,22] Both the number and size of the ctenoid plates increase with the size of the theca (taken as an indicator of ontogenetic stage in other non-radial echinoderms[23]) (Table S1), suggesting that the ctenidium grew through two distinct processes, plate addition and plate accretion, like the skeleton in living echinoderms.[24] We find that the ctenidium grew in a very similar way to ambulacra (Figure 2), characterized by the von Bertalanffy curve, with new plates added along rays from distinct growth zones (i.e., terminal addition[17]). In at least some ctenocystoids, the ctenidium encloses a pair of narrow grooves located on either side of the suroral plate, which are comparable to the ambulacral grooves seen in other echinoderms.[14–16]

There are substantial differences in the arrangement and morphology of the ctenidial plates compared with typical echinoderm ambulacral plate series, arguing against the homology of the ctenidium with specific axial elements such as brachioles (contra David et al.[15]). These include the apparent absence of floor plates and notable variability in the number and size of supposedly opposing plates enclosing the ambulacral grooves.[25] The ctenocystoid suroral plate, dorsal roof, and paired grooves have previously been inferred to be homologous with the cinctan operculum, labrum, and marginal groove(s)[21,25,26] (Figure 3B), allowing us to identify ambulacra in cinctans and pointing to their existence in members of all known extinct and extant echinoderm classes.[22] This allows us to establish clear axial homologies between bilateral, asymmetrical, and radial echinoderms, informing our phylogenetic analyses.

We find strong support for the placement of *Atlascystis* and other non-pentaradial fossil taxa as stem-group echinoderms (Figure 3A), revealing the evolution of the phylum through successive bilateral, asymmetrical, triradial, and pentaradial stages. These results argue against previous suggestions that non-radial forms are derived echinoderms[15,16,22] but agree with several recent quantitative analyses.[27–29] We reconstruct the most recent common ancestor of echinoderms as having possessed a tentacular feeding system derived from the left and right hydrocoels (Figure 3A), like extant pterobranch hemichordates.[30,31] *Ctenoimbricata*, recovered as sister to all other echinoderms, is characterized by a ctenidium in which the dorsal ctenoid plates (which partly enclose the ambulacral rays in *Atlascystis* and other ctenocystoids) are reduced to very small spinose plates,[21] raising doubts over whether this taxon possessed ambulacra. It is therefore possible that the ctenidium of *Ctenoimbricata* accommodated tentacular extensions of a water vascular system that were not directly associated with a specific plate series, with ambulacra first evolving in ctenocystoids like *Atlascystis*. In both *Ctenoimbricata* and *Atlascystis*, four suboral plates form the central part of the ventral ctenidium, indicating this was the plesiomorphic state for echinoderms. All ctenocystoids have two bilaterally symmetrical ambulacra, whereas cinctans include forms with an asymmetrical pair of left and right ambulacra (e.g., *Trochocystites*) or one (left) ambulacrum (e.g., *Protocinctus*) (Figure 3C). Consequently, the transition from ctenocystoids to cinctans involved the acquisition of strong left-right asymmetry, which may have been associated with the suppression of the right hydrocoel and, in cinctans with a single ambulacrum, the evolution of an ambulacral system derived from just the left hydrocoel (like extant echinoderms)[5,26,31] (Figure 3A). The presence of two ambulacra is likely the plesiomorphic state for cinctans, with the reduction of the ambulacral

Please cite this article in press as: Woodgate et al., A new Cambrian stem-group echinoderm reveals the evolution of the anteroposterior axis, Current Biology (2025), https://doi.org/10.1016/j.cub.2025.05.065

CellPress
OPEN ACCESS

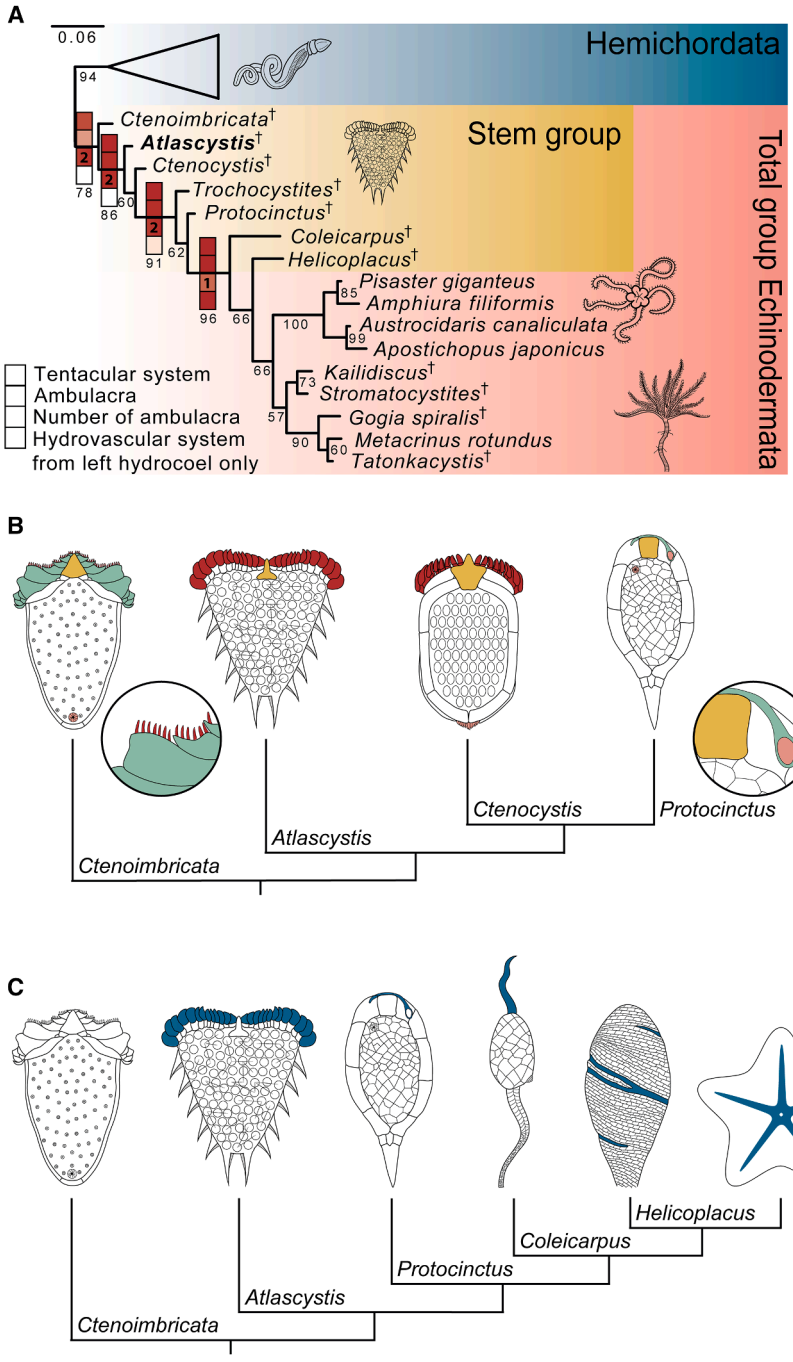

Figure 3. Phylogenetic position of *Atlascystis* and other echinoderms

(A) Majority-rule consensus tree from Bayesian phylogenetic analyses with ancestral state reconstructions for key characters (colors show probability of presence, with red equal to 1 and white equal to 0). Posterior probabilities are shown at resolved nodes. Fossil taxa indicated with a dagger symbol.

(B) Plate homologies (shown in different colors) between the fossil echinoderms *Ctenoimbricata*, *Atlascystis*, *Ctenocystis*, and *Protocinctus*, following Zamora et al.[21]

(C) Ambulacra (shown in blue) in the fossil echinoderms *Atlascystis* (two), *Protocinctus* (one), *Coleicarpus* (one), and *Helicoplacus* (three) and in an extant asteroid (five). *Ctenoimbricata* is reconstructed as having lacked ambulacra. Reconstructions are not shown to scale.

See also Figure S4 and Data S2.

system to a single ambulacrum occurring within a grade of cinctans. This implies that the right ambulacrum of ctenocystoids was completely lost during early echinoderm evolution, with their left ambulacrum homologous to the solute ambulacrum. This single ambulacrum gave rise to the three ambulacra of *Helicoplacus* and the five ambulacra of pentaradial echinoderms (Figure 3C), probably through duplication.[32,33]

Interpretation of the ctenidium as a pair of ambulacra informs a new hypothesis for the anteroposterior (A-P) patterning of *Atlascystis* and other ctenocystoids. Recent work examining the expression of conserved ectodermal A-P markers in the asteroid *Patiria miniata* suggests that in extant echinoderms the most anterior marker genes are expressed along the midline of each ambulacrum, with the more posterior anterior markers expressed laterally[10] (Figure 4B). We propose that in ctenocystoids the anteriormost genes were expressed in the ectoderm covering the ctenoid plates (which correspond to the ambulacral rays), while the more posterior anterior genes may have been expressed on the lateral sides of the ctenidium ectoderm (Figures 4C and 4D). The *Hox* genes involved in patterning the posterior trunk ectoderm in extant enteropneust hemichordates[34,35] (Figure 4A) and other bilaterians[36] are only expressed in the endoderm and mesoderm in *Patiria miniata*,[10] indicating that, from an ectoderm patterning perspective, extant echinoderms are mostly head-like animals. In contrast to living echinoderms, however, the bilateral symmetry exhibited by *Atlascystis* is more similar to the body plans of hemichordates and chordates. Morphofunctional comparisons with other extinct and extant deuterostomes suggest that the ctenocystoid theca accommodated a pharynx,[21,25] which corresponds to the anterior limit of *Hox* expression in hemichordates.[34,35] Taken together, this suggests that these ectodermal patterning genes were likely expressed posterior to the ctenidium and that the ctenocystoid theca is homologous to the hemichordate trunk (Figures 4A and 4C).

Our new hypothesis for A-P patterning in ctenocystoids (Figure 4) suggests a scenario for how this patterning program was modified during the early evolution of echinoderms. A key

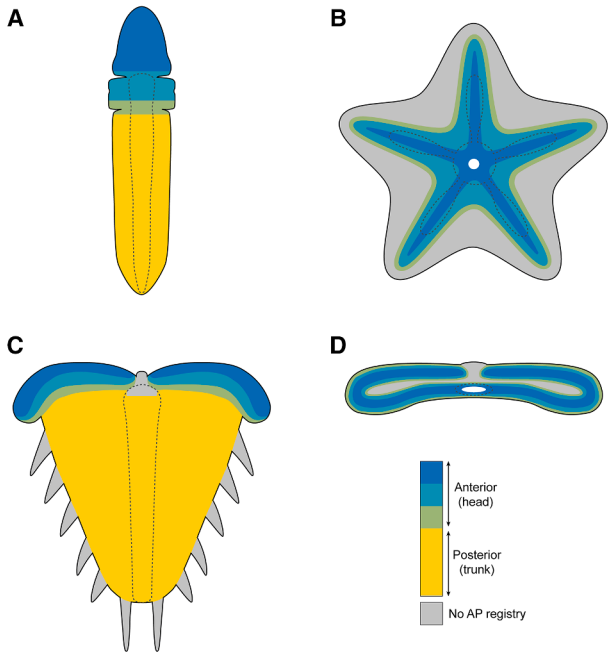

Figure 4. Anteroposterior patterning in *Atlascystis* and other deuterostomes

(A) Diagram showing A-P patterning in the extant enteropneust hemichordate *Saccoglossus kowalevskii* in dorsal view.

(B) Diagram showing A-P patterning in the extant asteroid *Patiria miniata* in oral view.

(C and D) Diagrams showing hypothesized A-P patterning in *Atlascystis acantha* in dorsal and oral views, respectively.

Dashed lines indicate the position of the digestive tract.

first step toward pentaradiality involved the establishment of left-right asymmetry in the ambulacra. In extant deuterostomes, a suite of signaling molecules under the control of Nodal plays an important role in patterning left-right asymmetry, inhibiting the formation of the right hydrocoel in larval sea urchins.[37,38] Therefore, variations in the left-right asymmetry of the ambulacra in ctenocystoids, cinctans, and solutes may be underpinned by changes to the deployment of the same developmental pathway. Because each ambulacrum was generated from a growth zone following the ocular plate rule,[17] the duplication of a single ambulacrum to give three ambulacra in helicoplacoids and, later, five ambulacra in pentaradial echinoderms was probably associated with duplication of the growth zone via an increase in the number of signaling centers responsible for plate addition. Our reconstruction of the A-P axis in *Atlascystis* indicates that ambulacral growth occurred far away from the posterior end of the body in ctenocystoids. Moreover, gene expression data for extant echinoderms demonstrate that no posterior markers are expressed in the ambulacra.[10] Together, this argues against the homology of these signaling centers with the bilaterian posterior growth zone (contra Byrne et al.[39]). The absence of trunk-like *Hox* expression in the ectoderm of extant echinoderms implies that the posterior registry was lost during the assembly of the phylum-level body plan.[10,40] By inferring *Hox* expression posterior to the ctenidium in *Atlascystis*, our hypothesis indicates that this loss happened after the divergence of ctenocystoids and all other echinoderms. We suggest this likely preceded the first radial forms, in which there is no evidence of a pharynx or any other morphological structures that could suggest the presence of a posterior territory. The loss of a trunk region in radial echinoderms could have enabled the duplication of ambulacra by releasing constraints on the development of anterior structures.

The transition from bilateral to pentaradial symmetry in echinoderms has long proved controversial.[6] Until now, the paucity of characters unambiguously uniting radial and non-radial fossil forms had hampered efforts to investigate the early evolution of the phylum. Our novel data on growth in the bilaterally symmetrical echinoderm *Atlascystis* confirm the presence of ambulacra in non-radial echinoderms, establishing homologies between all known fossil groups and enabling rigorous analyses of their phylogenetic relationships. The results allow us to uncover how ambulacra evolved in the echinoderm stem group, helping reconcile the phylum's rich early fossil record[5] with a robust new developmental model[10] and thereby decipher the early evolution of the A-P axis. *Atlascystis* and other ctenocystoids fill the morphological gulf between the ancestral deuterostome and extant echinoderms, revealing the acquisition of derived characters (i.e., ambulacra) alongside the retention of plesiomorphic features (i.e., a trunk). This reinforces the critical importance of the fossil record for elucidating the evolutionary assembly of animal body plans.

RESOURCE AVAILABILITY

Lead contact

Further information and requests for resources should be directed to and will be fulfilled by the lead contact, Imran A. Rahman (imran.rahman@nhm.ac.uk).

Materials availability

Newly described fossil specimens are located in the Natural History Museum, London (NHMUK).

Data and code availability

- Slices from synchrotron tomography and micro-CT scans, 3D models, the R script used for analyses of plate growth, and the character matrix used for phylogenetic analyses, are available from Zenodo: https://www.doi.org/10.5281/zenodo.15473979.
- This paper does not report original code.
- Any additional information required to reanalyze the data reported in this paper is available from the lead contact upon request.

ACKNOWLEDGMENTS

We thank National Geographic for funding fieldwork and Andrew Smith and Tim Ewin for assistance collecting specimens. We are grateful to the Paul Scherrer Institut, Villigen, Switzerland, for the provision of synchrotron radiation beamtime on the TOMCAT beamline at the Swiss Light Source; Pablo Villanueva Perez for support with synchrotron tomography; Russell Garwood and Alan Spencer for assistance with processing data; and Brett Clark and Eleanor Wilson for carrying out micro-CT scans. We also thank Tim Ewin, Giles Miller, and Hugh Carter for facilitating access to museum specimens; James Weaver and Lara Tomholt for providing the 3D model of *Pisaster giganteus* for analysis; Lucy Jackson for sharing images that informed the reconstruction of *Atlascystis* in Figure 3; and Chris Lowe for discussions of echinoderm evolutionary developmental biology. F.S.D. acknowledges support from the Natural Environment Research Council (NE/W00786X/1). J.T. was supported by a Leverhulme Trust Early Career Fellowship. S.Z. acknowledges support from the Spanish Ministry of Science and Innovation (PID2021-125585NB-I00), co-financed by the European Regional Development Fund, and the project "Aragosaurus: Recursos Geológicos y Paleoambientales" (E18_17R) funded by the

Government of Aragón. We are grateful to Graham Budd, Jakob Vinther, Brad Deline, and an anonymous reviewer for comments on an earlier version of this paper. This is a contribution to the Natural History Museum's Evolution of Life Research Theme.

AUTHOR CONTRIBUTIONS

I.A.R. designed the study. S.Z. collected and prepared the specimens. S.Z. and I.A.R. imaged the specimens. S.C.W. reconstructed the 3D model. S.C.W., S.Z., and I.A.R. described and interpreted the specimens. S.C.W. carried out the analyses of growth patterns. F.S.D. carried out the phylogenetic analyses. J.R.T., L.F., and I.A.R. interpreted the development of early echinoderms. S.C.W., F.S.D., and I.A.R. prepared the figures. I.A.R. wrote the first draft of the manuscript. All authors reviewed and edited the manuscript.

DECLARATION OF INTERESTS

The authors declare no competing interests.

STAR★METHODS

Detailed methods are provided in the online version of this paper and include the following:

- KEY RESOURCES TABLE
- EXPERIMENTAL MODEL AND STUDY PARTICIPANT DETAILS
  - Material
- METHOD DETAILS
  - Nomenclatural acts
  - Imaging
- QUANTIFICATION AND STATISTICAL ANALYSIS
  - Quantifying plate growth
  - Phylogenetic analyses
  - Bayes factor test
  - Ancestral state reconstructions

SUPPLEMENTAL INFORMATION

Supplemental information can be found online at https://doi.org/10.1016/j.cub.2025.05.065.

Received: February 20, 2025
Revised: April 25, 2025
Accepted: May 29, 2025

REFERENCES

1. Peterson, K.J., Arenas-Mena, C., and Davidson, E.H. (2000). The A/P axis in echinoderm ontogeny and evolution: evidence from fossils and molecules. Evol. Dev. *2*, 93–101. https://doi.org/10.1046/j.1525-142x.2000.00042.x.
2. Smith, A.B. (2008). Deuterostomes in a twist: the origins of a radical new body plan. Evol. Dev. *10*, 493–503. https://doi.org/10.1111/j.1525-142X.2008.00260.x.
3. David, B., and Mooi, R. (2014). How Hox genes can shed light on the place of echinoderms among the deuterostomes. EvoDevo *5*, 22. https://doi.org/10.1186/2041-9139-5-22.
4. Nanglu, K., Cole, S.R., Wright, D.F., and Souto, C. (2023). Worms and gills, plates and spines: the evolutionary origins and incredible disparity of deuterostomes revealed by fossils, genes, and development. Biol. Rev. Camb. Philos. Soc. *98*, 316–351. https://doi.org/10.1111/brv.12908.
5. Rahman, I.A., and Zamora, S. (2024). Origin and early evolution of echinoderms. Annu. Rev. Earth Planet. Sci. *52*, 295–320. https://doi.org/10.1146/annurev-earth-031621-113343.
6. Hyman, L.H. (1955). The Invertebrates: Echinodermata. The Coelomate Bilateria*4* (McGraw-Hill).
7. Nielsen, C. (2012). Animal Evolution: Interrelationships of the Living Phyla (Oxford University Press).
8. Giribet, G., and Edgecombe, G.D. (2020). The Invertebrate Tree of Life (Princeton University Press). https://doi.org/10.1515/9780691197067.
9. Smith, A.B., Zamora, S., and Álvaro, J.J. (2013). The oldest echinoderm faunas from Gondwana show that echinoderm body plan diversification was rapid. Nat. Commun. *4*, 1385. https://doi.org/10.1038/ncomms2391.
10. Formery, L., Peluso, P., Kohnle, I., Malnick, J., Thompson, J.R., Pitel, M., Uhlinger, K.R., Rokhsar, D.S., Rank, D.R., and Lowe, C.J. (2023). Molecular evidence of anteroposterior patterning in adult echinoderms. Nature *623*, 555–561. https://doi.org/10.1038/s41586-023-06669-2.
11. Geyer, G., and Landing, E. (2004). A unified Lower – Middle Cambrian chronostratigraphy for West Gondwana. Acta Geol. Pol. *54*, 179–218.
12. Peng, S., Babcock, L.E., and Cooper, R.A. (2012). The Cambrian period. In The Geologic Time Scale 2012, F.M. Gradstein, J.G. Ogg, M. Schmitz, and G. Ogg, eds. (Elsevier), pp. 437–488. https://doi.org/10.1016/B978-0-444-59425-9.00019-6.
13. Álvaro, J.J., Esteve, J., and Zamora, S. (2018). Morphological assessment of the earliest paradoxidid trilobites (Cambrian Series 3) from Morocco and Spain. Geol. Mag. *155*, 1566–1595. https://doi.org/10.1017/S0016756817000449.
14. Sprinkle, J., and Robison, R.A. (1978). Addendum to subphylum Homalozoa. Ctenocystoids. In Treatise on Invertebrate Paleontology, Part T: Echinodermata 2, Crinoidea, R.C. Moore, and C. Teichert, eds. (University of Kansas and The Geological Society of America), pp. T998–T1002.
15. David, B., Lefebvre, B., Mooi, R., and Parsley, R. (2000). Are homalozoans echinoderms? An answer from the extraxial-axial theory. Paleobiology *26*, 529–555. https://doi.org/10.1666/0094-8373(2000)026<0529:AHEAAF>2.0.CO;2.
16. Mooi, R., Lefebvre, B., Guensburg, T.E., Nohejlová, M., and Dupichaud, C. (2024). Approaches to understanding echinoderm origins. Part 2: questioning conceptual models. Cah. Biol. Mar. *65*, 463–490.
17. Mooi, R., David, B., and Wray, G.A. (2005). Arrays in rays: terminal addition in echinoderms and its correlation with gene expression. Evol. Dev. *7*, 542–555. https://doi.org/10.1111/j.1525-142X.2005.05058.x.
18. von Bertalanffy, L. (1938). A quantitative theory of organic growth (inquiries on growth laws. II). Hum. Biol. *10*, 181–213.
19. Moss, D.K., Ivany, L.C., and Jones, D.S. (2021). Fossil bivalves and the sclerochronological reawakening. Paleobiology *47*, 551–573. https://doi.org/10.1017/pab.2021.16.
20. Zachos, L.G. (2009). A new computational growth model for sea urchin skeletons. J. Theor. Biol. *259*, 646–657. https://doi.org/10.1016/j.jtbi.2009.04.007.
21. Zamora, S., Rahman, I.A., and Smith, A.B. (2012). Plated Cambrian bilaterians reveal the earliest stages of echinoderm evolution. PLoS ONE *7*, e38296. https://doi.org/10.1371/journal.pone.0038296.
22. Sumrall, C.D., and Wray, G.A. (2007). Ontogeny in the fossil record: diversification of body plans and the evolution of "aberrant" symmetry in Paleozoic echinoderms. Paleobiology *33*, 149–163. https://doi.org/10.1666/06053.1.
23. Zamora, S., Rahman, I.A., and Smith, A.B. (2013). The ontogeny of cinctans (stem-group Echinodermata) as revealed by a new genus, *Graciacystis*, from the middle Cambrian of Spain. Palaeontology *56*, 399–410. https://doi.org/10.1111/j.1475-4983.2012.01207.x.
24. Smith, A.B. (2005). Growth and form in echinoids: the evolutionary interplay of plate accretion and plate addition. In Evolving Form and Function: Fossils and Development, D.E.G. Briggs, ed. (Yale Peabody Museum), pp. 181–195.
25. Rahman, I.A., and Clausen, S. (2009). Re-evaluating the palaeobiology and affinities of the Ctenocystoidea (Echinodermata). J. Syst. Palaeontol. *7*, 413–426. https://doi.org/10.1017/S1477201909990046.
26. Rahman, I.A., and Zamora, S. (2009). The oldest cinctan carpoid (stem-group Echinodermata), and the evolution of the water vascular system.

Zool. J. Linn. Soc. *157*, 420–432. https://doi.org/10.1111/j.1096-3642.2008.00517.x.

27. Topper, T.P., Guo, J., Clausen, S., Skovsted, C.B., and Zhang, Z. (2019). A stem group echinoderm from the basal Cambrian of China and the origins of Ambulacraria. Nat. Commun. *10*, 1366. https://doi.org/10.1038/s41467-019-09059-3.
28. Nanglu, K., Caron, J.-B., and Cameron, C.B. (2020). Cambrian tentaculate worms and the origin of the hemichordate body plan. Curr. Biol. *30*, 4238–4244.e1. https://doi.org/10.1016/j.cub.2020.07.078.
29. Li, Y., Dunn, F.S., Murdock, D.J.E., Guo, J., Rahman, I.A., and Cong, P. (2023). Cambrian stem-group ambulacrarians and the nature of the ancestral deuterostome. Curr. Biol. *33*, 2359–2366.e2. https://doi.org/10.1016/j.cub.2023.04.048.
30. Cameron, C.B. (2005). A phylogeny of the hemichordates based on morphological characters. Can. J. Zool. *83*, 196–215. https://doi.org/10.1139/z04-190.
31. Smith, A.B. (2005). The pre-radial history of echinoderms. Geol. J. *40*, 255–280. https://doi.org/10.1002/gj.1018.
32. Hotchkiss, F.H.C. (1998). A "rays-as-appendages" model for the origin of pentamerism in echinoderms. Paleobiology *24*, 200–214. https://doi.org/10.1666/0094-8373(1998)024[0200:AMFTOO]2.3.CO;2.
33. Isaeva, V.V., and Rozhnov, S.V. (2022). Transformation of the ancestral body plan and axial growth in echinoderms: ontogenetic and paleontological data. Paleontol. J. *56*, 863–886. https://doi.org/10.1134/S0031030122080032.
34. Lowe, C.J., Wu, M., Salic, A., Evans, L., Lander, E., Stange-Thomann, N., Gruber, C.E., Gerhart, J., and Kirschner, M. (2003). Anteroposterior patterning in hemichordates and the origins of the chordate nervous system. Cell *113*, 853–865. https://doi.org/10.1016/s0092-8674(03)00469-0.
35. Gonzalez, P., Uhlinger, K.R., and Lowe, C.J. (2017). The adult body plan of indirect developing hemichordates develops by adding a Hox-patterned trunk to an anterior larval territory. Curr. Biol. *27*, 87–95. https://doi.org/10.1016/j.cub.2016.10.047.
36. Swalla, B.J. (2006). Building divergent body plans with similar genetic pathways. Heredity *97*, 235–243. https://doi.org/10.1038/sj.hdy.6800872.
37. Duboc, V., Röttinger, E., Lapraz, F., Besnardeau, L., and Lepage, T. (2005). Left-right asymmetry in the sea urchin embryo is regulated by Nodal signaling on the right side. Dev. Cell *9*, 147–158. https://doi.org/10.1016/j.devcel.2005.05.008.
38. Smith, M.S., Turner, F.R., and Raff, R.A. (2008). Nodal expression and heterochrony in the evolution of dorsal–ventral and left–right axes formation in the direct-developing sea urchin *Heliocidaris erythrogramma*. J. Exp. Zool. B Mol. Dev. Evol. *310*, 609–622. https://doi.org/10.1002/jez.b.21233.
39. Byrne, M., Martinez, P., and Morris, V. (2016). Evolution of a pentameral body plan was not linked to translocation of anterior Hox genes: the echinoderm HOX cluster revisited. Evol. Dev. *18*, 137–143. https://doi.org/10.1111/ede.12172.
40. Adachi, S., Niimi, I., Sakai, Y., Sato, F., Minokawa, T., Urata, M., Sehara-Fujisawa, A., Kobayashi, I., and Yamaguchi, M. (2018). Anteroposterior molecular registries in ectoderm of the echinus rudiment. Dev. Dyn. *247*, 1297–1307. https://doi.org/10.1002/dvdy.24686.
41. Tomholt, L., Baum, D., Wood, R.J., and Weaver, J.C. (2023). High-throughput segmentation, data visualization, and analysis of sea star skeletal networks. J. Struct. Biol. *215*, 107955. https://doi.org/10.1016/j.jsb.2023.107955.
42. Schneider, C.A., Rasband, W.S., and Eliceiri, K.W. (2012). NIH Image to ImageJ: 25 years of image analysis. Nat. Methods *9*, 671–675. https://doi.org/10.1038/nmeth.2089.
43. Sutton, M.D., Garwood, R.J., Siveter, D.J., and Siveter, D.J. (2012). SPIERS and VAXML; a software toolkit for tomographic visualisation and a format for virtual specimen interchange. Palaeontol. Electron. *15*, 5T.
44. Blender Development Team. (2023). Blender, [Version 3.5]. https://www.blender.org.
45. Comet Technologies Canada Inc. (2022). Dragonfly, [Version 2022.2]. https://www.theobjects.com/dragonfly.
46. R Core Team (2023). R: a Language and Environment for Statistical Computing (R Foundation for Statistical Computing). https://www.Rproject.org.
47. Ronquist, F., Teslenko, M., van der Mark, P., Ayres, D.L., Darling, A., Höhna, S., Larget, B., Liu, L., Suchard, M.A., and Huelsenbeck, J.P. (2012). MrBayes 3.2: efficient Bayesian phylogenetic inference and model selection across a large model space. Syst. Biol. *61*, 539–542. https://doi.org/10.1093/sysbio/sys029.
48. Huson, D.H., and Bryant, D. (2024). The SplitsTree App: interactive analysis and visualization using phylogenetic trees and networks. Nat. Methods *21*, 1773–1774. https://doi.org/10.1038/s41592-024-02406-3.
49. Zamora, S., Álvaro, J.J., Clausen, S., and Esteve, J. (2014). Open quarry of the Brèche à Micmacca Member crossing the "telesto level" at Assemame, central Anti-Atlas. In Stratigraphic Overview of the Ediacaran and Cambrian from the Anti Atlas, Morocco, L. Devaere, S. Clausen, and J.J. Álvaro, eds. (Université Lille 1), pp. 72–75.
50. Geyer, G., Landing, E., and Heldmaier, W. (1995). Faunas and depositional environments of the Cambrian of the Moroccan Atlas regions. In Morocco. Beringeria Special Issue 2: '95 – The Lower-Middle Cambrian Standard of western Gondwana, G. Geyer, and E. Landing, eds. (Würzburg: Institut für Paläontologie der Universität Würzburg), pp. 47–119.
51. Stampanoni, M., Groso, A., Isenegger, A., Mikuljan, G., Chen, Q., Bertrand, A., Henein, S., Betemps, R., Frommherz, U., Böhler, P., et al. (2006). Trends in synchrotron-based tomographic imaging: the SLS experience. Proc. SPIE *6318*, U199–U212. https://doi.org/10.1117/12.679497.
52. Brombacher, A., Searle-Barnes, A., Zhang, W., and Ezard, T.H.G. (2022). Analysing planktonic foraminiferal growth in three dimensions with foram3D: an R package for automated trait measurements from CT scans. J. Micropalaeontol. *41*, 149–164. https://doi.org/10.5194/jm-41-149-2022.
53. Arnhold, E. (2017). easynls: Easy Nonlinear Model. https://CRAN.R-project.org/package=easynls.
54. Beverton, R.J.H., and Holt, S.J. (1957). On the Dynamics of Exploited Fish Populations (Springer).
55. Gulland, J.A. (1973). Manual of Methods for Fish Stock Assessment. Part 1. Fish Population Analysis (Food and Agriculture Organization of the United Nations).
56. Ogle, D.H., and Isermann, D.A. (2017). Estimating age at a specified length from the von Bertalanffy growth function. N. Am. J. Fish. Manag. *37*, 1176–1180. https://doi.org/10.1080/02755947.2017.1342725.
57. Bell, B.M. (1976). Phylogenetic implications of ontogenetic development in the class Edrioasteroidea (Echinodermata). J. Paleontol. *50*, 1001–1019.
58. Hotchkiss, F.H.C. (2012). Growth zones and extraxial-axial skeletal homologies in Asteroidea (Echinodermata). Proc. Biol. Soc. Wash. *125*, 106–121. https://doi.org/10.2988/11-37.1.
59. Lewis, P.O. (2001). A likelihood approach to estimating phylogeny from discrete morphological character data. Syst. Biol. *50*, 913–925. https://doi.org/10.1080/106351501753462876.
60. Xie, W., Lewis, P.O., Fan, Y., Kuo, L., and Chen, M.-H. (2011). Improving marginal likelihood estimation for Bayesian phylogenetic model selection. Syst. Biol. *60*, 150–160. https://doi.org/10.1093/sysbio/syq085.

Please cite this article in press as: Woodgate et al., A new Cambrian stem-group echinoderm reveals the evolution of the anteroposterior axis, Current Biology (2025), https://doi.org/10.1016/j.cub.2025.05.065

CellPress
OPEN ACCESS

STAR★METHODS

KEY RESOURCES TABLE

REAGENT or RESOURCE	SOURCE	IDENTIFIER
Deposited data		
Character matrix	This study	Zenodo: https://www.doi.org/10.5281/zenodo.15473979
Digital model of the Cambrian ctenocystoid *Atlascystis acantha*	This study	Zenodo: https://www.doi.org/10.5281/zenodo.15473979
Digital model of the Cambrian ctenocystoid *Ctenocystis utahensis*	This study	Zenodo: https://www.doi.org/10.5281/zenodo.15473979
Digital model of the extant echinoid *Austrocidaris canaliculata*	This study	Zenodo: https://www.doi.org/10.5281/zenodo.15473979
Digital model of the extant asteroid *Pisaster giganteus*	Tomholt et al.[41]	https://doi.org/10.1016/j.jsb.2023.107955
Software and algorithms		
ImageJ v. 1.50	Schneider et al.[42]	https://imagej.net/ij/
SPIERS v. 3.0.0	Sutton et al.[43]	https://github.com/palaeoware/SPIERS
Blender v. 3.5	Blender Development Team[44]	https://www.blender.org
Dragonfly v. 2022.2	Comet Technologies Canada Inc.[45]	https://www.theobjects.com/dragonfly
R	R Core Team[46]	https://www.R-project.org
MrBayes v. 3.2.7	Ronquist et al.[47]	https://nbisweden.github.io/MrBayes/index.html
SplitsTree App v. 6.0.01	Huson and Bryant[48]	https://github.com/husonlab/splitstree6
Other		
Fossil specimens	Natural History Museum, London (NHMUK)	NHMUK EE 19394, 15319, 15324a, 15325, 15428, 19395–19399

EXPERIMENTAL MODEL AND STUDY PARTICIPANT DETAILS

Material

Fossil specimens of *Atlascystis acantha*, preserved as molds coated with iron oxides, were collected from the Brèche à Micmacca Member of the Jbel Wawrmast Formation, which corresponds to the Agdzian regional stage, approximately equivalent to the Stage 4–Wuliuan boundary interval, Cambrian Series 2–Miaolingian. Specimens came from two localities (Assemame and Tarhouch 3) in the Anti-Atlas, Morocco. The Assemame locality (31.28768°N 4.98493°W) is located at Assemame quarry, near Alnif. It exposes a complete section of the Jbel Wawrmast Formation, including both the Brèche à Micmacca and Tarhoucht members. Fossil echinoderms, including edrioasteroids, stylophorans, *Helicocystis*, and ctenocystoids, are relatively abundant in loose boulders derived from the 'telesto level', which is thought to belong to the *Morocconus notabilis* Zone based on the associated trilobites.[13,49] The Tarhouch 3 locality (31.39459°N, 5.01977°W) is located on the northern slope of Bou Tiouit hill, 1 km southwest of Tarhoucht and 13 km south of Tinejdad. Here, the sampled levels occur in a series of quarries from which trilobites are collected. These levels are equivalent to those described in Geyer et al.[50] and the associated fauna of trilobites is indicative of the *Morocconus notabilis* Zone. Specimens are housed at the Natural History Museum, London (NHMUK).

METHOD DETAILS

Nomenclatural acts

This published work and the nomenclatural acts it contains have been registered in ZooBank, the online registration system for the International Commission on Zoological Nomenclature (ICZN). The Life Science Identifier (LSID) for this publication is: urn:lsid:zoobank.org:pub:46A97BED-436A-4F7D-BC04-14293BBADF3A.

Imaging

Specimens of *Atlascystis acantha* were cast in latex four or five times to remove the iron oxides and thereby provide an accurate representation of the original skeletal morphology. The final casts were whitened with NH_4Cl sublimate and photographed.

The holotype (NHMUK EE 19394) was imaged with synchrotron tomography using the TOMCAT beamline of the Swiss Light Source, Paul Scherrer Institut, Villigen, Switzerland.[51] The fossil was scanned in six blocks at 1.25x optical magnification, using

Please cite this article in press as: Woodgate et al., A new Cambrian stem-group echinoderm reveals the evolution of the anteroposterior axis, Current Biology (2025), https://doi.org/10.1016/j.cub.2025.05.065

an X-ray energy of 37 keV, 1001 projections per block and an exposure time of 1000 ms per projection. Slices were reconstructed with in-house software, using a custom algorithm to reduce ring artefacts. This gave a tomographic dataset consisting of 2495 slices with a voxel size of about 5.2 μm. Slices were cropped and processed in ImageJ v. 1.50[42] to remove background noise. This involved the following steps: (1) the 'Find Edges' function was applied to the original slices, thresholded images were created from these processed images, and the 'Dilate' function was applied to the thresholded images; (2) the 'Invert' function was applied to the dilated thresholded images; (3) the original slices and the images from (1) were combined using the 'AND' function; (4) a median filter (radius = 4 pixels) was applied to the original slices and the results were combined with the images from (2) using the 'AND' function; and (5) the images from (3) and (4) were combined using the 'ADD' function. This processed dataset was then digitally reconstructed as a virtual fossil using SPIERS v. 3.0.0.[43] Here, an inverted linear threshold was used to create binary images with all pixels darker than a user-defined gray-level turned 'on'. Pixels identified as belonging to the fossil were manually assigned to distinct regions-of-interest (e.g. different plates), which were then rendered as separate isosurfaces to give a three-dimensional (3-D) model of the fossil. To minimize noise, weak smoothing and island removal were applied to the model. Lastly, high-quality images were rendered in Blender v. 3.5.[44]

To facilitate comparative analyses of plate growth, an adult specimen (NHMUK 1936.9.1.41-42) of the extant echinoid *Austrocidaris canaliculata* was imaged with micro-CT using a Nikon XT H 225 cabinet scanner at the Natural History Museum, London. The specimen was scanned together with five other echinoids using a 3 mm thick copper filter, 200 kV voltage, 160 μA current, and 1800 projections (each with an exposure time of 500 ms). Tomographic reconstruction was performed in Nikon CT Pro software using filtered back projection, giving a tomographic dataset consisting of 2225 slices with a voxel size of about 34.6 μm. The scan data for NHMUK 1936.9.1.41-42 was cropped out from the full dataset prior to further analysis. This dataset was visualized as a 3-D model using Dragonfly v. 2022.2.[45]

QUANTIFICATION AND STATISTICAL ANALYSIS

Quantifying plate growth

Digital reconstructions of the Cambrian ctenocystoids *Atlascystis acantha* (this study) and *Ctenocystis utahensis*,[25] the extant echinoid *Austrocidaris canaliculata* (this study), and the extant asteroid *Pisaster giganteus*[41] were used to measure plate dimensions and extract centroid coordinates (Data S1). In *Atlascystis* and *Ctenocystis*, the centroid coordinates of the ctenoid plates were computed in Blender based on the center of mass relative to the surface. In *Austrocidaris*, the centroid coordinates of the ambulacral plates were computed following segmentation of the ambulacral pores in Dragonfly. In *Pisaster*, the centroid coordinates of the ambulacral plates were estimated in Blender by using a primitive shape (a singular isolated plate scaled to approximately the same size, orientation, and location as the target ambulacral plate) to mark the positions of the 20 proximal-most plates, the 20 distal-most plates, and each 10th plate in between those. Plate lengths (perpendicular to the axis of growth, see Figure S3) were measured in Blender and then scaled to the length of the largest plate in each taxon to remove the effects of specimen size. The centroid coordinates were used to calculate the distance from the proposed site of addition (adjacent to the suroral plate in the ctenocystoids, the ocular plates in *Austrocidaris*, and the terminal podia in *Pisaster*) for each plate using the package foram3D[52] in R.[46] We inferred that the ctenoid plates were added on either side of the suroral plate in ctenocystoids because: (i) the ctenoid plates progressively change in size and shape ventrolaterally, indicating that they form part of the same series of plates; and (ii) the number of ctenoid plates increases with the size of the theca (taken as an indicator of ontogenetic stage[23]) (Table S1), demonstrating that plates were added during growth. The measured distances from the sites of addition were then scaled to the furthest distance from the site of addition in each taxon to remove the effects of specimen size.

For each taxon, the fit to a von Bertalanffy growth curve was determined using the R package easynls.[53] A von Bertalanffy curve was selected due to its general ability to link length to growth stage in vertebrates and invertebrates; this function is commonly used to estimate age based on body length in fish[54–56] and aquatic invertebrates (see Moss et al.[19] and references there-in), and it also describes the addition of plates according to the ocular plate rule in echinoids.[20] More broadly, echinoderm ambulacra grow in accordance with the ocular plate rule; however, with the exception of some edrioasteroids[57] and derived eleutherozoans,[20,58] non-ambulacral plates (which are not characterized by terminal addition from a specific growth zone) do not follow this rule.[17] Consequently, if plate growth fits a von Bertalanffy curve this provides a strong indication that these structures grew according to the ocular plate rule and is suggestive of their interpretation as ambulacra. The starting iteration coefficient values were specified based on lines plotted using the abline function in R (*A. acantha*: a = 0.3, b = 0.45; *C. utahensis*: a = 0.33, b = 0.72; *A. canaliculata*: a = 0.65, b = 0.19; *P. giganteus*: a = 0.44, b = 0.58; c = 0.8 for all taxa) and used to generate a function with coefficients minimizing the residual sum of squares value (Table S2).

Phylogenetic analyses

Phylogenetic analyses were performed using a revised version of the matrix from Li et al.[29] with nine new or replacement taxa (additional fossil echinoderms to better represent the known disparity of Cambrian echinoderms) and 38 new characters (to capture the morphologies of these new fossil taxa), giving a total of 68 taxa and 368 characters. The matrix uses named species for all fossils and extant echinoderms, with hypothetical generic organisms used to represent enteropneust families, chordate subphyla, and non-deuterostome bilaterian phyla. A complete description of the characters is provided in Data S2.

Phylogenetic analyses were performed in MrBayes v. 3.2.7[47] under the Mkinf + gamma model.[59] Because the matrix includes autapomorphies and invariant characters and sampling was non-exhaustive, analyses were set to correct for the ascertainment

Please cite this article in press as: Woodgate et al., A new Cambrian stem-group echinoderm reveals the evolution of the anteroposterior axis, Current Biology (2025), https://doi.org/10.1016/j.cub.2025.05.065

(coding) bias, ensuring that only parsimony-informative characters were included. A gamma distribution was used to model rate variation, with transition rate symmetry, and a compound Dirichlet prior on branch lengths. Two independent runs of four chains were run for 10,000,000 generations or until convergence was reached, sampling every 100 generations, and with 25% of trees removed as burnin. Convergence was assessed based on the effective sample size (ESS) (>200), potential scale reduction factor (PRSF) (~1.000), and the average standard deviation of split frequencies (<0.01). The results were summarized as a majority-rule consensus tree (Figure S4A).

To test if the recovered topology was sensitive to the choice of how to model rate variation, we also ran analyses using a log-normal model of rate variation (Figure S4B). In addition, to explore the sensitivity of our results to the inclusion of discrete characters referring to the presence or absence of specific genes (which cannot be scored in any fossils), we repeated our analyses with these characters (316–342) excluded (Figure S4C). To visualize the uncertainty in our phylogenetic analyses, we used the SplitsTree App v. 6.0.01[48] to produce a consensus network summarizing the posterior distribution of 5288 trees from both runs (excluding 25% discarded as burnin), with the threshold percentage for node recovery set at 10% (Figure S4D).

Bayes factor test

We used a Bayes factor test to evaluate the support for our phylogeny (H_0) versus an alternative hypothesis[16] (H_1). First, we generated two different trees in MrBayes using hard constraints to force the topology to match either H_0 or H_1. These constraints are provided in Data S2. Then, we used the stepping-stone method[60] to estimate the marginal likelihood of H_0 against H_1, running analyses for both these trees with 50 steps, each with 17,500,000 generations (>10 times the number required to reach convergence in our main analyses). Two independent runs were performed for each hypothesis. Lastly, the Bayes factor support ($2 \times \log_e$ BF) was calculated based on the mean marginal likelihoods for H_0 and H_1 (Table S3).

Ancestral state reconstructions

Ancestral state reconstructions of all 368 characters were performed in MrBayes. To accommodate phylogenetic uncertainty, we used the command 'report ancstates' after placing hard monophyly constraints on our nodes of interest: (1) total-group echinoderms; (2) all echinoderms except *Ctenoimbricata*; (3) all echinoderms except *Ctenoimbricata*, *Atlascystis*, and *Ctenocystis*; and (4) all echinoderms except *Ctenoimbricata*, *Atlascystis*, *Ctenocystis*, *Trochocystites*, and *Protocinctus*. These constraints are provided in Data S2. Convergence was assessed based on the effective sample size (>200).